INVESTIGATION OF SPUTTERED $Ba_{0.5}Sr_{0.5}Co_{0.8}Fe_{0.2}O_{3-\delta}$ ELECTRODES WITH IMPEDANCE SPECTROSCOPY

by

Andrew Baker

A thesis submitted to the Faculty of the University of Delaware in partial fulfillment of the requirements for the degree of Bachelor of Mechanical Engineering with Distinction.

Spring 2011

INVESTIGATION OF SPUTTERED

$Ba_{0.5}Sr_{0.5}Co_{0.8}Fe_{0.2}O_{3-\delta}$ ELECTRODES

WITH IMPEDANCE SPECTROSCOPY

by

Andrew Baker

Approved: _____

Joshua Hertz, Ph.D.
Professor in charge of thesis on behalf of the Advisory Committee

Approved: _____

Suresh Advani, Ph.D.
Committee member from the Department of Mechanical Engineering

Approved: _____

Victor Kaliakin, Ph.D.
Committee member from the Board of Senior Thesis Readers

Approved: _____

Donald Sparks, Ph.D.
Chair of the University Committee on Student and Faculty Honors

ACKNOWLEDGMENTS

There are many people I would like to thank for their support. First, I would like to thank my advisor, Dr. Joshua Hertz for giving me the opportunity to perform research in his lab. He provided me with my first research experience in the summer of 2009 and has provided me with invaluable guidance since then. Additionally, I would like to thank my second and third readers Dr. Suresh Advani and Dr. Victor Kaliakin for their assistance and support in completing this thesis.

I would also like to thank my fellow Hertz Group members, especially James White for help with the x-ray diffractions and Philip Zandona for help with the finicky sputtering machine. Also, I would like to thank Mr. Steve Beard for all of his help in the machine shop, and for putting up with all of my broken mill bits; Dr. David Burris for the use of the optical interferometry and Dr. Raul Lobo for use of the x-ray diffractometer.

Finally, I would like to thank my family who has helped foster my creativity and desire to learn. To my parents Rita and Jim my sister Lauren, I am extremely grateful for your endless support and love.

TABLE OF CONTENTS

LIST OF TABLES

LIST OF FIGURES

ABSTRACT

Solid oxide fuel cells (SOFCs) are energy conversion devices that rely upon the oxidation of a hydrogen-based fuel to generate electricity. They are extremely attractive for use in automotive and stationary power because of their high efficiency compared to combustion engines and broad range of fuels which can be used. Currently, performance of SOFCs is hindered by one or more rate-limiting steps at the cathode of the fuel cell. By replacing traditional porous, electron conducting cathode materials with those capable of mixed ionic/electronic conduction (known as MIECs), efficiency can be greatly increased.

This work focused on the synthesis and characterization of the MIEC known as BSCF. This material was synthesized in the bulk using traditional solid state ceramic processing methods and its crystal structure was verified using x-ray diffraction. Sputtering deposition rates were then performed under a variety of processing parameters and optical interferometry was used to measure the thickness of the resulting films. It was shown that optimal film growth occurred at a sputtering power of 75 W with a pressure of 5 mTorr and an $Ar:O_2$ ratio of 8:2. BSCF was then deposited into 200 nm thick, circular electrodes ranging from 1 to 5 mm in diameter on a yttria-stabilized zirconia (YSZ) substrate (the industry standard for SOFC electrolytes).

Initial impedance spectroscopy measurements were taken on this system to quantify its performance in an SOFC system. Based on the results, it is proposed that

one or more factors caused inconsistencies in the data. Therefore, multiple methods are proposed to improve the electrode processing method as well as impedance spectroscopy techniques.

Chapter 1

INTRODUCTION AND BACKGROUND

1.1 Fuel Cell Relevance

Fuel cells are energy conversion devices that produce electricity by reacting a fuel, such as hydrogen, with an oxidant, such as air through an electrochemical reaction. These devices consist of two electronically conductive electrodes: an anode and a cathode, which are separated by an electrolyte which is ionically conductive, yet electronically insulating[1]. When the hydrogen is oxidized, the resulting electrons are forced from the anode through the load back to the cathode to reduce the oxygen which completes the circuit.

The most common types of fuel cells are known as proton exchange membrane fuel cells (PEMFCs). PEMFCs contain a membrane which conducts only protons from the anode to the cathode. While PEM fuel cells are becoming increasingly more popular, several drawbacks exist, such as inefficiency in operation at low temperature and use of expensive catalyst metals for production[1].

1.2 Solid Oxide Fuel Cells

Currently being researched are solid oxide fuel cells (SOFCs) which rely on solid-state ceramic components for operation. These components have the ability to efficiently conduct electrons and/or ions and can be manufactured from inexpensive

precursor materials. Because of these benefits, SOFCs are an appealing replacement for PEMFCs.

One of the drawbacks of SOFCs is the high temperature required for operation (traditionally >800°C). This temperature does, however, promote rapid reaction kinetics that allow for a hydrocarbon fuel to be reformed within the fuel cell and produces heat for use in cogeneration[1]. Because of this high operating temperature, SOFCs are being considered primarily for stationary power, auxiliary power or automotive applications.

1.1.1 SOFC Components

The main components of the SOFC include the electrolyte, anode and cathode (Figure 1.1):

Figure 1.1: Schematic diagram of the SOFC (Minh, *J. Am. Ceram. Soc.* 76, 565)

The purpose of the electrolyte is to conduct oxygen ions (O^{2-}) between the anode and the cathode. Thus the electrolyte must be highly conductive to O^{2-} while remaining electrically insulating. Currently, compounds such as yttria-stabilized zirconia (YSZ) and gadolinium-doped cerium oxide (CGD) are being used as electrolytes[1].

The anode and cathode must conduct electrons generated at the electrode/electrolyte interface through the outer circuit back to the cathode. The anode must be porous as well to diffuse the fuel to the interface as well as transport excess fuel and water out of the cell. Typically, SOFC anodes consist of a porous YSZ support structure coated in metal such as nickel or cobalt[1].

Cathodes must also be ionically conductive to transport the oxidant to the electrolyte. Because it is difficult for a component to exhibit electronic and ionic conduction, much of the inefficiency within the SOFC is attributed to rate-limiting steps in the cathode. Because of this, research has focused on improving ionic and electronic conduction in the cathode to improve efficiency of the SOFC.

1.1.2 Cathode Structure and Performance

Most SOFC cathodes exist in one of two forms: a porous electron conductor or a composite made from separate electron and ion-conducting materials. Porous electron conductors rely on diffusion of oxygen through the pores of the membrane itself to transport oxygen gas to the interface. In these systems, the reaction is limited to the triple phase boundary (TPB), which is the area where the oxidant, the cathode and the electrolyte come into contact. In order to improve ionic conductivity and expand the reaction area beyond a planar TPB, composite electronic-ionic conduction materials are being developed. These materials consist of an

interpenetrating network of electron and ion conducting materials, such as metals and YSZ, respectively.

Composites such as Pt-YSZ have been used to improve upon traditional porous cathodes[2]. Recently, a new class of materials is being studied which could further improve the efficiency of SOFC cathodes. These materials are known as mixed ionic/electronic conductors (MIECs). MIECs conduct both ions and electrons, meaning the reaction area is significantly improved to the entire free surface of the MIEC.

1.2 BSCF

Barium strontium cobalt ferrite, or BSCF, is a type of ceramic MIEC which relies on its perovskite crystal structure for its conductive properties. The perovskite crystal structure is represented by the formula ABO_3. Where the A represents the A-site cation with a charge of 2+ and the B represents the B-site cation with a charge of 4+ (Figure 1.2). The cations are balanced by three oxygen anions with a charge of 2- each. BSCF is formed by combining barium and strontium at the A-site and cobalt and iron at the B-site yielding $Ba_xSr_{1-x}Co_yFe_{1-y}O_{3-\delta}$ (where $0 < x,y < 1$).

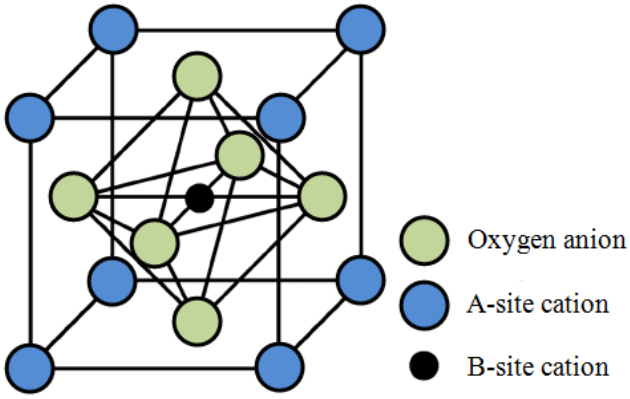

Figure 1.2: The ABO_3-type perovskite crystal structure

Particularly promising is the compound $Ba_{0.5}Sr_{0.5}Co_{0.8}Fe_{0.2}O_{3-\delta}$ which is the most thoroughly studied of the BSCF compounds due to its optimal conductive properties[3] (Figure 1.3). Therefore, this stoichiometry of BSCF will be investigated in this work.

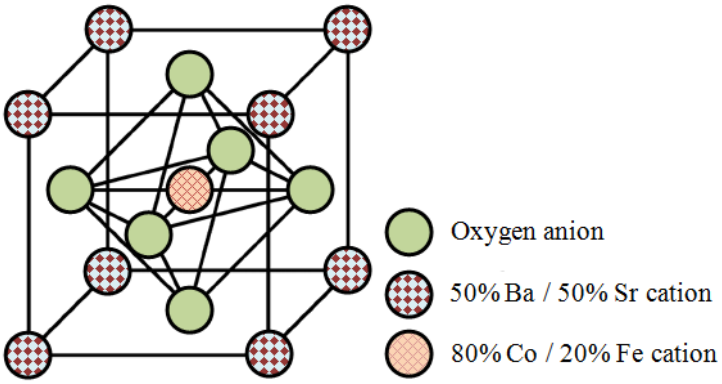

Figure 1.3: The perovskite crystal structure and composition of BSCF

1.3 Impedance Spectroscopy

Impedance spectroscopy is frequently used to quantify electrochemical processes of SOFC components. Specifically, this method can be used to determine how well a ceramic cathode can conduct electrons and oxide ions (O^{2-}), which directly correlates to its performance in an SOFC. In this technique, AC voltage is applied to a sample at varying frequencies and the resultant current is measured. The data is typically plotted as the real vs. imaginary impedance and fit to an equivalent circuit. This circuit consists of a configuration of resistors and/or capacitors, which relate to impedances in electron and ion conductivity at different areas of the system (such as the free surfaces, the bulk and the interfaces).

1.3.1 Data Analysis

Plotting the imaginary and real impedance at each frequency usually yields one or more semicircles. These impedances, Z_R and Z_C, respectively, correspond to resistive (R) and capacitive (C) elements n the system (shown in Equations 1 and 2):

$$Z_R = R \qquad (1)$$

$$Z_C = (i\omega C)^{-1} \qquad (2)$$

It is typical for constant phase elements (CPEs) to be applied to a circuit as well, which involves introducing an exponent to the denominator of the capacitive impedance. The exponent n (Equation 3) in the CPE can be used to account for inhomogeneities within the system such as impurities or irregular grain boundary alignment, which results in flattened, or depressed, semi-circles in the data set[2].

$$Z_Q = (Q(i\omega)^n)^{-1} \qquad (3)$$

Depending on the value of the exponent, the CPE can behave as a resistor (n = 0), inductor (n = -1) or capacitor (n = 1). It is important to note that the exponent should be >0.8 in order to ensure that element is describing a "capacitive" electrochemical process. Often it is difficult to fit data with equivalent circuits because of the infinite nature of possible circuit configurations. Because multiple circuit configurations can have equivalent impedances, the researcher must have a good understanding of the system to support the elements in the equivalent circuit. From this constant phase element, Q, the capacitance can be calculated[4] (Equation 4):

$$C = (R^{1-n}Q)^{1/n} \quad (4)$$

Recently, there has been great interest in studying thin electrodes. By depositing the electrodes as thin, geometrically-defined entities, it can be assumed that bulk ionic resistance is negligible. Therefore, the impedance spectra can be used to identify the magnitude and contributions of other rate limiting steps within the system.

1.3.1 Impedance Spectroscopy of BSCF

Baumann, et. al have rigorously derived an equivalent circuit for thin, oxygen-deficient perovskite materials using a simplified version of the drift-diffusion model[4]. Baumann has identified three key features in the impedance spectra of these materials: the high frequency (HF) axis intercept, the medium frequency (MF) arc and the low frequency (LF) arc. The HF axis intercept occurs along the real resistance (Z') axis and corresponds to the ohmic resistance of the bulk YSZ electrolyte (R_b). The MF arc occurs after the HF axis intercept. From this arc, the interfacial resistance to ionic transfer (R_i) and boundary capacitance due to interfacial stoichiometric change (C_i) can be determined. The final feature is the LF arc which describes resistance

associated with O_2 exchange at the electrode surface (R_s) as well as chemical capacitance in the bulk due to stoichiometric changes (C_{chem}).

Figure 1.4: Resistor/capacitor network for MIECs (Baumann, et. al., *Solid State Ionics* 117, 3187)

Figure 1.5: Impedance spectroscopy data for BSCF deposited through PLD. (Baumann, et. al.*, Solid State Ionics* 117, 3187)

This model has been used to describe the processes in LSCF and BSCF deposited through pulse laser deposition[4,5] (PLD). This circuit will be initially used in this work to initially quantify the performance of BSCF thin films deposited through sputtering.

1.4 Sputter Deposition

Sputtering is a form of physical vapor deposition that relies on bombarding a target of bulk material with argon ions to eject a vapor of that material. The vapor is then re-condensed onto a substrate, forming a thin film. The thickness and atomic structure of the film that forms on this substrate is a function of the processing parameters of the deposition such as substrate temperature and rotation, and deposition environment gas composition. In this experiment, reactive sputtering

was used as the primary means of depositing BSCF thin films, which means the BSCF target was deposited in an environment of argon and oxygen in order to grow an oxide film on the substrate.

One of the major goals of this experiment is to compare the performance of sputter-deposited films of BSCF and those deposited through PLD. Because sputtering does not require the use of a laser, films can be created more inexpensively than through PLD. If the performance is similar, sputtering can be suggested as an attractive method for mass-producing BSCF cathode components.

Chapter 2

MATERIALS AND METHODS

The goal of this research was to characterize the ceramic barium strontium cobalt ferrite (BSCF). This will be accomplished by synthesizing bulk BSCF in bulk form and subsequently depositing and characterizing thin films of the material. These thin films will have implications as cathodes in μSOFCs. Here, bulk BSCF was synthesized using traditional solid state ceramic processing methods and its crystal structure and purity was characterized using x-ray diffraction (XRD). Then, sputtering was used to deposit thin (<1 μm) films of BSCF onto silicon (Si) and yttria-stabilized zirconia (YSZ) substrates. Optical interferometry was used to determine the deposition rate of the sputtered films and XRD was again used to investigate the crystal phase of the films. Finally, impedance spectroscopy was used to characterize the electrochemical performance of the films.

2.1 Target Fabrication

Solid state powder processing was used to create bulk BSCF powder[6]. The carbonates of barium and strontium and the oxides of iron (III) and cobalt (II,III) were weighed in the correct stoichiometric ratio needed create $Ba_{0.5}Sr_{0.5}Co_{0.8}Fe_{0.2}O_{3-\delta}$ (Table 2.1).

Table 2.1: Theoretical relative mass fractions of each compound necessary to create bulk BSCF

Compound	Mass Fraction
$BaCO_3$	0.3905
$SrCO_3$	0.2921
Co_3O_4	0.2541
Fe_2O_3	0.0632

This specific composition was chosen to match what has been used in prior reports[3,5]. The precursor powders were ball milled with 5 mm YSZ milling media for 24 hours in deionized (DI) water to thoroughly mix the powders. The YSZ beads were removed and the suspension was dried using a conventional hotplate. The powder was then calcined at 1000°C for 2 hours and again at 1100°C for 5 hours to completely react the precursor powders. Between each of the calcining steps, XRD was used to verify the crystal phase of the powder.

Next, the calcined powder was ball milled with YSZ balls and 1 weight percent polyvinyl acetate (PVA), a binding agent, in DI water for 24 hours. The suspension was again dried using a conventional hotplate. The calcined powder/PVA mixture was placed in a 64 mm (~2.5 in) stainless steel die (Figure A.1) lubricated with stearic acid and compressed to 170 MPa (5,000 lbs) for 5 minutes to create a disc approximately 10 mm thick with a diameter of 64 mm. This green body was then sintered in an environment of flowing O_2 at 1300°C for 5 hours to consolidate it into a dense disk for use as a sputtering target. A chip of the sintered target was broken off and XRD'd to ensure it too had the proper phase.

2.2 Phase Verification

X-ray powder diffraction (XRD) was used as the primary method to verify the perovskite crystal phase of the BSCF after each of the processing stages (Figure

A.2). X-rays were produced with copper anode ($\lambda \approx 1.54$ Å). Measurements were taken with a continuous scan ranging from 10° to 80° with a step size of 0.02° and an integration time of 1.5 seconds per step.

2.3 Thin Film Processing

After creation and phase characterization of the BSCF target using powder processing and XRD techniques, it was loaded into the main chamber of the sputtering system (Figure A.3) which is held continuously in high vacuum (<5e-7 Torr). The target was positioned over a magnetron sputtering gun, which used a radio frequency (RF) electric field over the surface of the target. The substrates were loaded into a substrate holder which was rotated at 30 RPM to ensure uniform film growth. During the deposition process, Ar and O_2 gasses are flowed into the chamber at a specific ratio programmed into mass flow controllers (MFCs). The overall gas pressure in the chamber was measured in the chamber using a manometer and held constant by varying the pumping speed with a programmable gate valve. The flow rate of Ar and O_2 gasses was kept constant through all experiments at a total of 20 sccm. The ratio of Ar to O_2 flow rates was controlled as desired for a particular deposition experiment. As power is applied to the gun, a plasma forms on the surface of the target, which energizes and traps Ar^+ ions. These energetic ions bombarded the surface of the target, causing the target material to vaporize within the chamber. Since the guns were aimed at the rotating substrates, this vapor condensed on the substrate, growing a thin film.

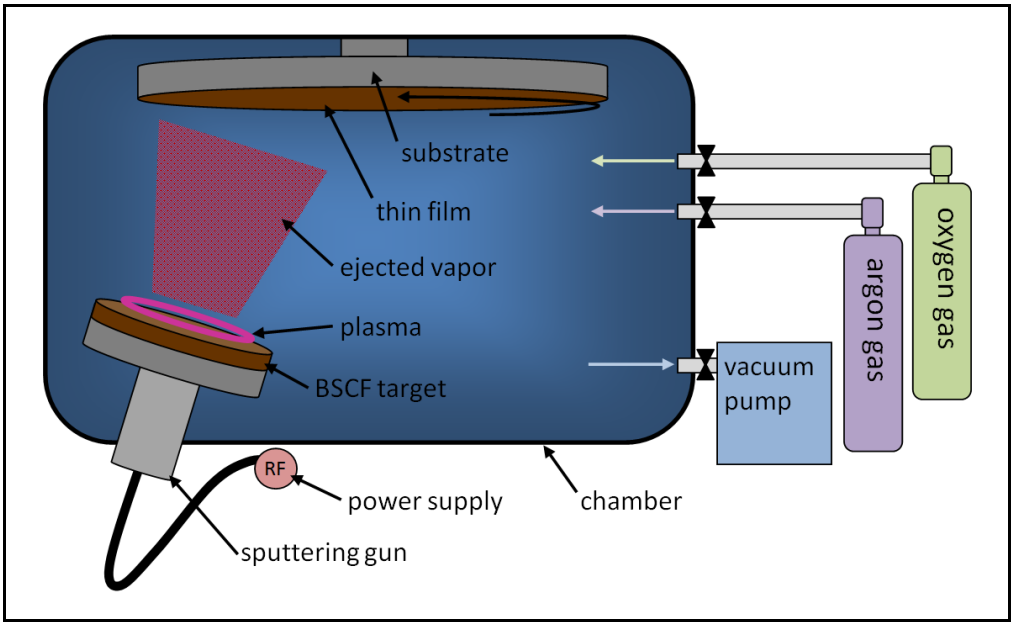

Figure 2.1: Diagram of sputtering process

2.4 Deposition Rate Measurement

As previously noted, sputtering process parameters can affect the characteristics of the deposited thin film such as the thickness and morphology. These parameters include the temperature of the substrate upon which the film is deposited, the power applied to the target, the pressure of sputtering gasses within the chamber and the ratio of reactive gasses to inert gasses within the chamber (Ar to O_2). In this experiment, the latter three parameters were varied to investigate the deposition of BSCF.

In order to determine how varying these parameters affect the deposition rate of BSCF, the ceramic was deposited under a matrix of different processing parameters. This was carried out by first cleaning a 10 x 10 x 0.5 mm Si substrate and masking half of it with vacuum tape (Figure A.4). Substrates were cleansed to remove

dust and organics by successively rinsing them with acetone, isopropanol, and DI water ("triple rinse") and then drying with high-pressure, filtered dry air. Next, BSCF was deposited on this substrate for 6 hours under a prescribed condition. The tape was removed after deposition to form a film step on bare silicon. The process was repeated for a variety of prescribed processing parameters. These parameters included powers of 25, 50 and 75 W; 9:1 and 8:2 ratios of $Ar:O_2$ gas compositions; and pressures of 5 and 10 mTorr. The samples were then triple rinsed and coated with ~40 nm titanium (50W DC, 10 mT, 100% Ar, 30 RPM substrate rotation, 1 hour) to create a reflective top surface necessary for optical interferometry.

Optical interferometry was used to measure step height created by the masked deposition, and thereby the thickness of the resultant films. The films were loaded onto the stage of the interferometer (Figure A.5). The interferometer generates a 1 x 1 mm surface profile of the film (Figure 2.2). From this surface profile, the number of pixels at each height can be counted and plotted in a histogram (Figure 2.3). In a step film, each region of the step will correspond to a peak on the histogram. Taking the difference between the heights of each peak will yield the height of the step, which is equal to the thickness of the film. Dividing the thickness of the film by the deposition time (here, 6 hours) yielded a deposition rate for each combination of processing parameters. Deposition rate was assumed, as is commonly found, to be constant with time.

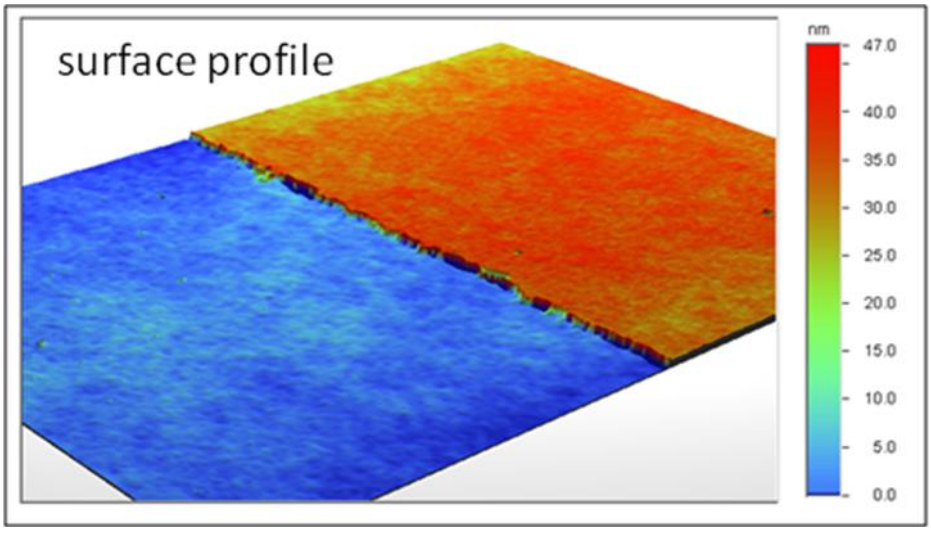

Figure 2.2: Example data showing a 1 x 1 mm surface profile measured by optical interferometry

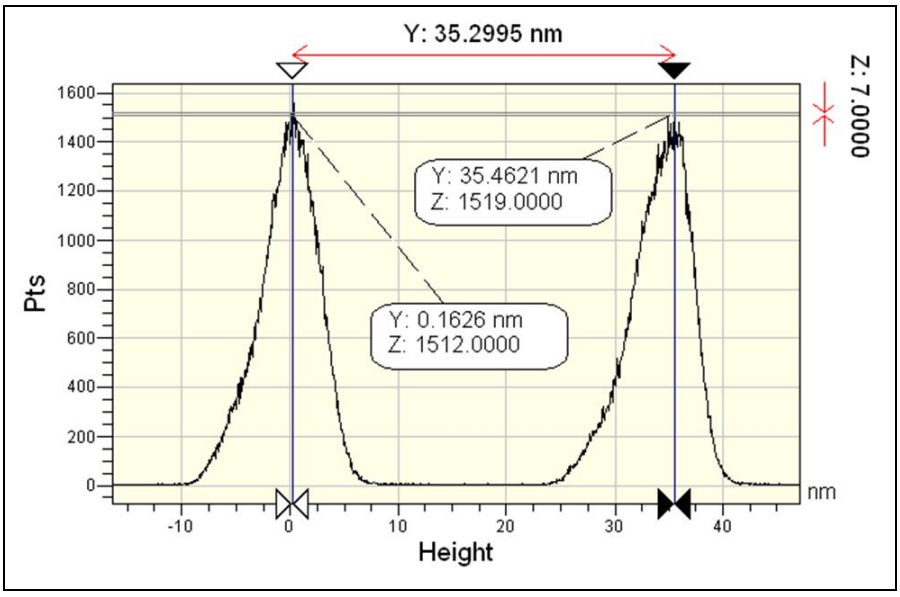

Figure 2.3: Example data showing the occurrence of pixels at each height in the surface profile

2.5 Electrode Fabrication

Once deposition rate was determined, BSCF could be fabricated into electrodes for testing in impedance spectroscopy. In order to create the electrodes, a mask was machined from 6061-T6 aluminum plate which would fit in a standard 4-inch (101.6 mm) wafer holder and allow specified film patterns to be deposited upon 10 x 10 mm square substrates (Figure 2.4).

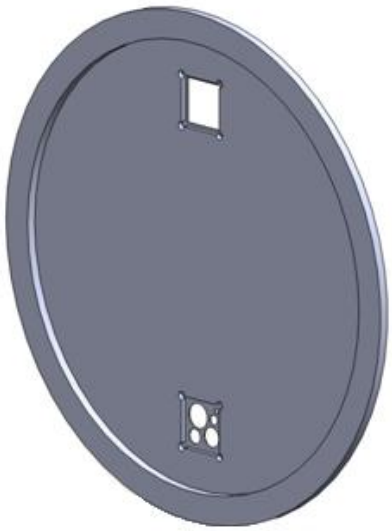

Figure 2.4: CAD model of sample mask (OD = 101.6 mm)

The mask contains holes ranging from 1 to 5 mm to create the front, or "working" electrodes and a 9.5 x 9.5 mm square cutout for creating the back, or "counter" electrode. The thickness of the mask is 0.125 mm (0.005 in) to reduce the aspect ratio of the features in order to reduce shadowing. This shadowing would reduce the deposition rate near the edges, possibly creating pores or other undesirable edge effects. Once the mask was created, a complete sample could be created in two

separate depositions: one to create the set of working electrodes, and one to create the counter electrode. BSCF was deposited onto 10 x 10 x 0.5 mm YSZ substrates (Coating and Crystal Technology) to create electrodes with a thickness of 200 nm.

2.6 Conductivity Measurement

Impedance spectroscopy was used as the primary method for determining conductivity of the sample electrodes (Figure A.6). In order to take measurements, two silver wire leads were threaded into two separate 2-bore alumina tubes (Figure 2.5). The first lead was silver pasted to the back electrode of the sample. The second lead was looped into the second bore, creating a loop. During measurements, the first lead/electrode assembly (with back electrode facing down) was lowered into the box furnace (Thermolyne 47900). The second looped lead was then lowered into the furnace to contact the front electrodes. The benefit of using two separate alumina tubes is that the front electrode contact could be manipulated while maintaining temperature of the furnace, allowing multiple electrodes to be measured without changing temperature. Measurements were taken on 5 and 3 mm samples at 600, 700 and 800°C

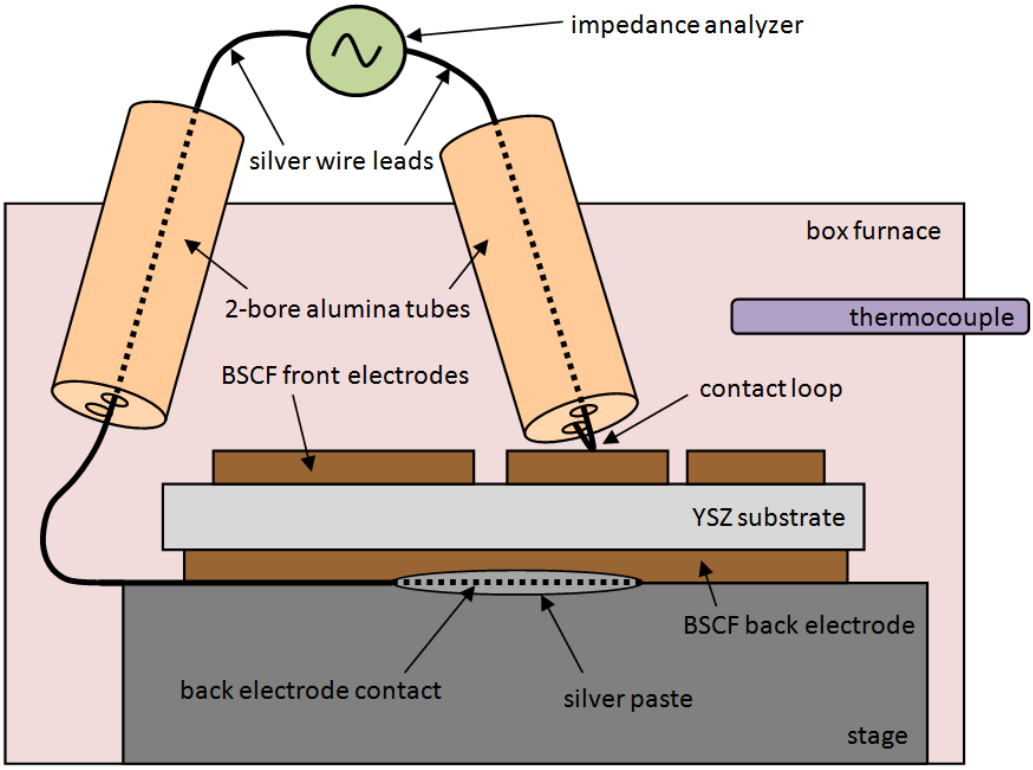

Figure 2.5: Schematic showing impedance spectroscopy measurement set-up

Chapter 3

RESULTS AND DISCUSSIONS

3.1 Target Fabrication

BSCF powder was successfully created using traditional solid state ceramic processing. After calcining BSCF powder, a sputtering target was successfully pressed yet initially, sintering in air at 1300°C for 5 hours yielded unfavorable results. The instability of BSCF with respect to changes in oxidation state led to considerable difficulty in fabrication of a dense target. This behavior has been noted by other researchers[8]. Initially, all thermal processing was performed in air and the resultant ceramic pieces were highly cracked and mechanically weak. It is believed that the target was reducing at high temperature and re-oxidizing upon cooling; the volume change associated with these reactions led to the observed behavior. Subsequent sintering steps were performed in flowing pure O_2 gas and resulted in a strong, dense target (Figure 3.1).

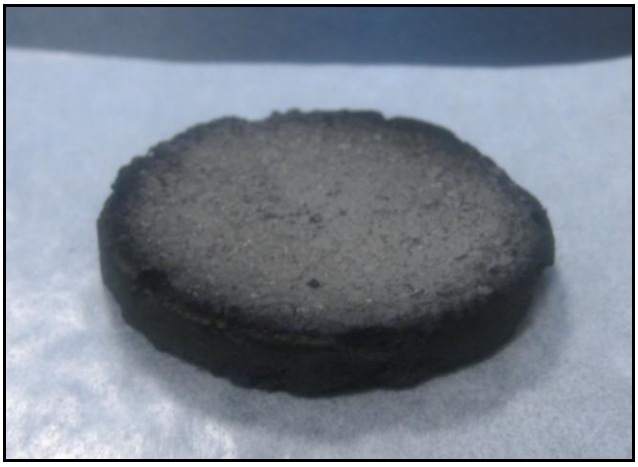

Figure 3.1: The 50 mm diameter BSCF sputtering target

3.2 Phase Verification

Throughout each of the processing steps, XRD was applied to verify material crystal phase was consistent with literature values[7] (Figure 3.2).

Figure 3.2: Literature x-ray diffraction pattern for BSCF (Wei, et. al., *Electrochem. Solid-State Lett*. 8, A428)

XRD was taken after calcining the BSCF powder at 1000°C for 2 hours (Figure 3.3, a). It can be seen that additional peaks occur (indicated by red arrows), suggesting the presence of $BaCoO_2$ impurities[7]. Further calcining the powder at 1100°C for 5 hours (b) successfully removed all impurities, leaving the correct perovskite crystal structure. After sintering at 1300°C for 5 hours (c), XRD showed that the material maintained the correct perovskite crystal structure.

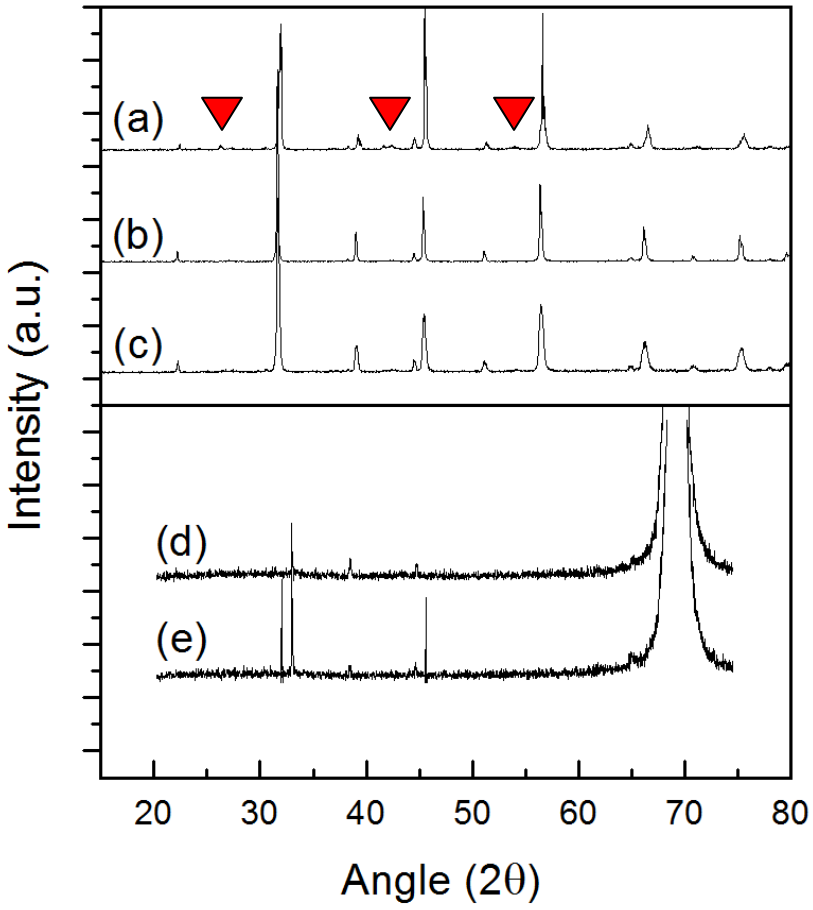

Figure 3.3: X-ray diffraction patterns for calcined (a,b) and sintered (c) BSCF, bare Si (d) and BSCF film on Si (e)

XRD was also taken on bare Si substrates (d) and compared to that of a 200 nm BSCF film on a Si substrate (e). Initially, it appears that there is no qualitative difference in XRD patterns of Si with or without a film. This could indicate that the film measured was simply too thin for the technique used and the perovskite peaks were lost in the noise of the measurement, or that the film is amorphous and indeed the thin film pattern is correct in showing that no peaks are present. In order to verify this, it is necessary to test thicker films or use glancing-angle XRD (GAXRD), a technique used to perform diffraction on thin films.

3.3 Film Deposition

Upon creation of the BSCF sputtering target, deposition rate measurement could begin. BSCF was deposited for 6 hours at RF powers of 25, 50 and 75 W with gas ratios of 9:1 and 8:2 Ar:O_2 and overall chamber pressures of 5 and 10 mTorr. The thicknesses of these films are tabulated (Table A.1) to determine the optimal processing parameters.

From the results (Figure 3.4), it can be seen that deposition increases as a function of power for each of the processing parameters, (with the exception of the 75 W, 10 mTorr, 8:2 Ar:O_2 deposition) which is consistent with expected results. Optimal deposition occurred at a power of 75 W with a chamber pressure of 5 mTorr containing 8:2 Ar:O_2. Now that processing parameters are now calibrated to specific film thickness, films of any thickness can be grown simply by varying the time of deposition.

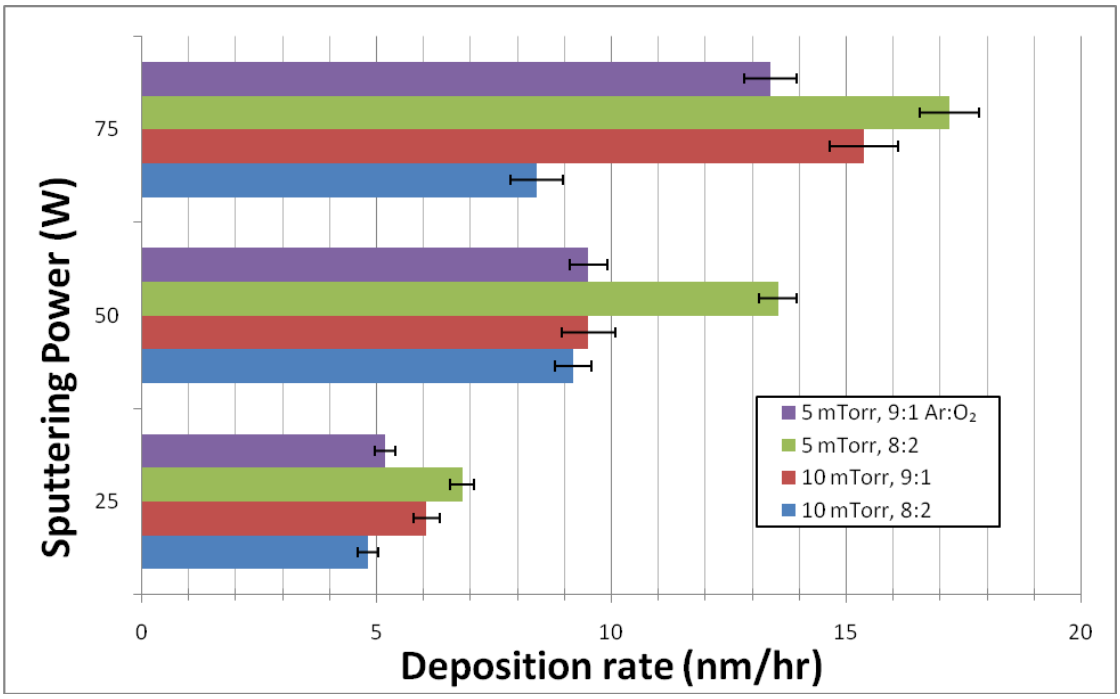

Figure 3.4: Deposition rate measurements of BSCF

3.4 Electrode Fabrication

Using the aluminum mask, 200 mm thick BSCF working electrodes with diameters of 1 to 5 mm were successfully sputtered onto a 10 x 10 mm YSZ substrate (Figure 3.5). A 9.5 x 9.5 mm square BSCF counter electrode was also deposited on the back side of this sample.

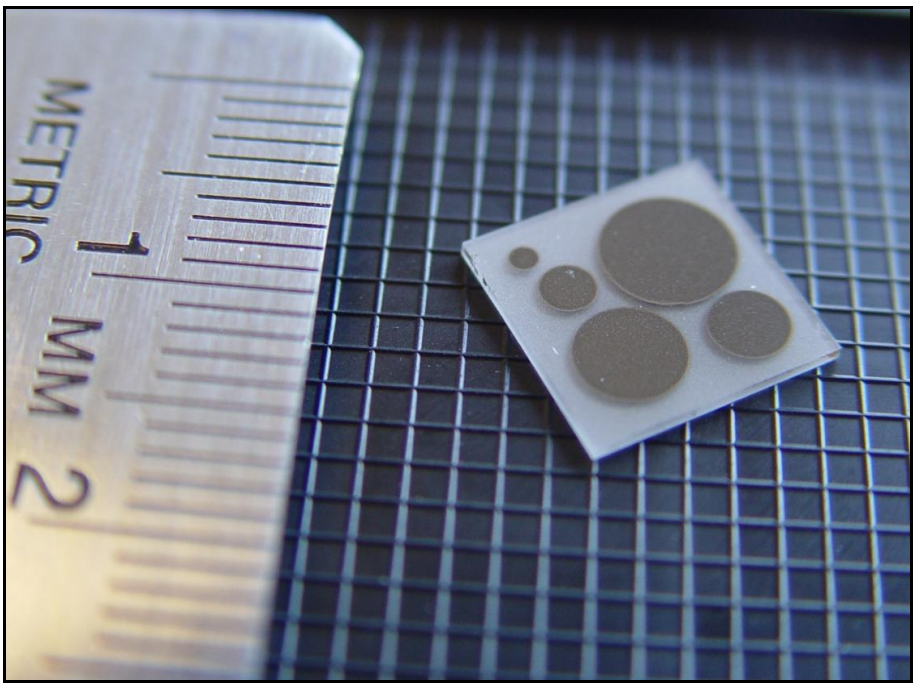

Figure 3.5: A 10 x 10 mm YSZ substrate with 200 nm thick, circular BSCF working electrodes, with diameters of 1 to 5 mm

3.5 Conductivity

Impedence spectroscopy measurements were taken on 5 and 3 mm samples at 600, 700 and 800°C (Figure 3.6). Because of their size, it was extremely difficult to align the 1 and 2 mm electrodes with the alumina contact manipulator.

Because of this difficulty, measurements were taken on the 5 and 3 mm electrodes alone to test the broadest possible range of electrode sizes. In order to contact the smaller electrodes, it is necessary to refine the measurement setup.

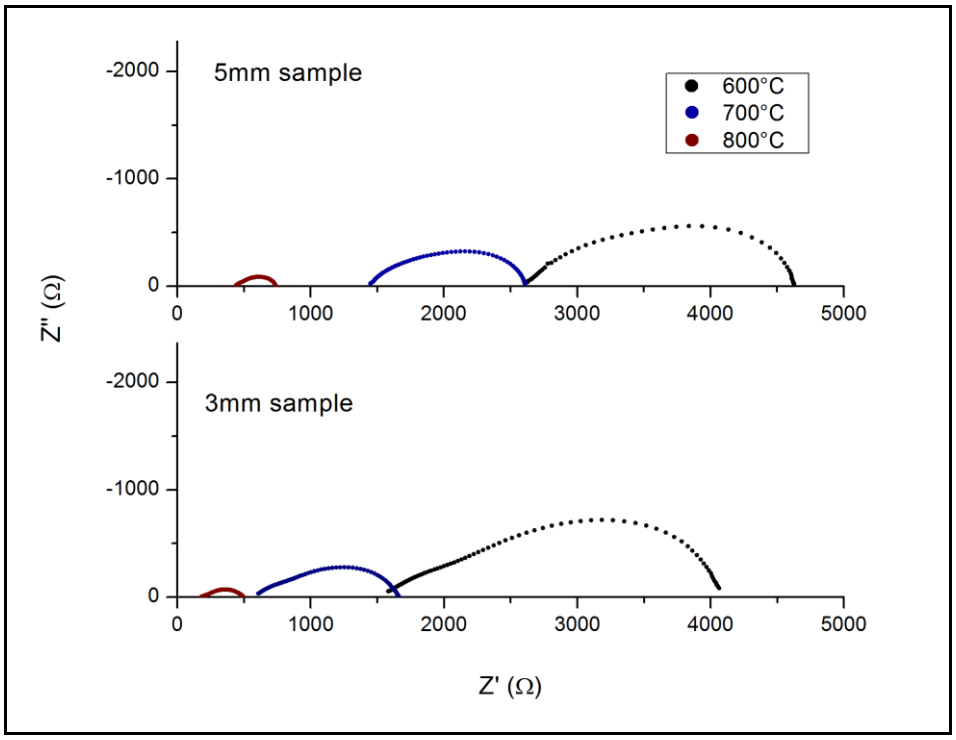

Figure 3.6: Impedance spectroscopy results for 5 mm and 3 mm samples at 600, 700 and 800°C

The R/C circuit previously used by Baumann[4] was initially fit to the data, but resultant fits were inaccurate. Therefore, a more universal circuit was applied. This circuit contained a resistor in parallel series with two parallel resistor-CPE pairs (Figure 3.7).

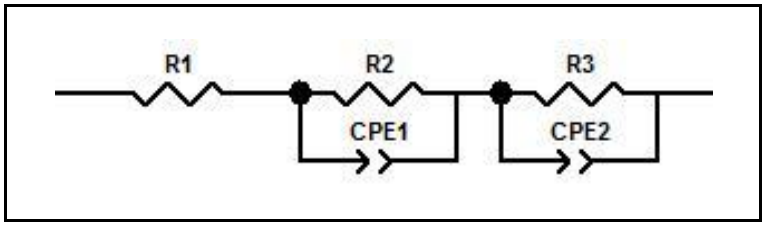

Figure 3.7: Universal circuit used for data fitting.

The first resistor corresponds to the x-axis intercept and relates to the impedance of the YSZ substrate. The two resistor-CPE pairs are intended to fit the two overlapping semi-circular features of the data set. An example fit to this circuit is shown (Figure 3.8).

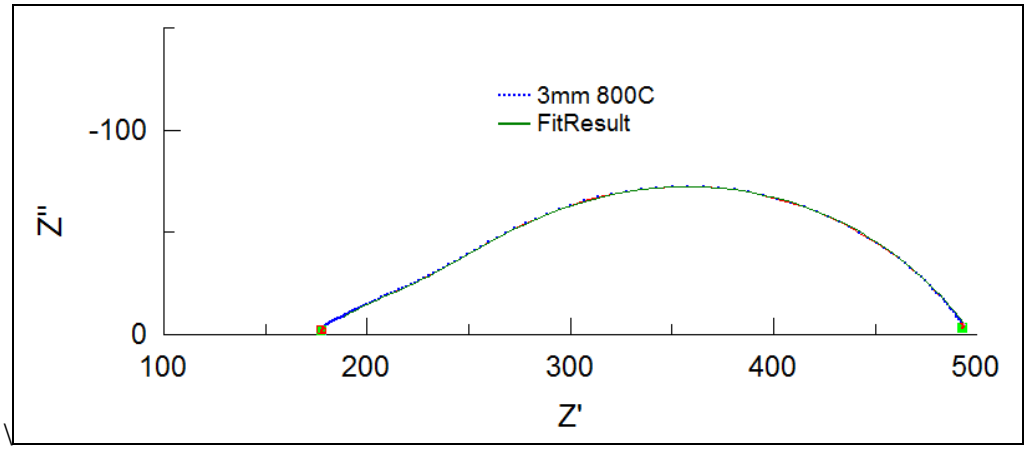

Figure 3.8: Fit results (green) for impedance data of 3 mm sample at 800°C (blue)

Graphing the data (Table A.2) yields the following results:

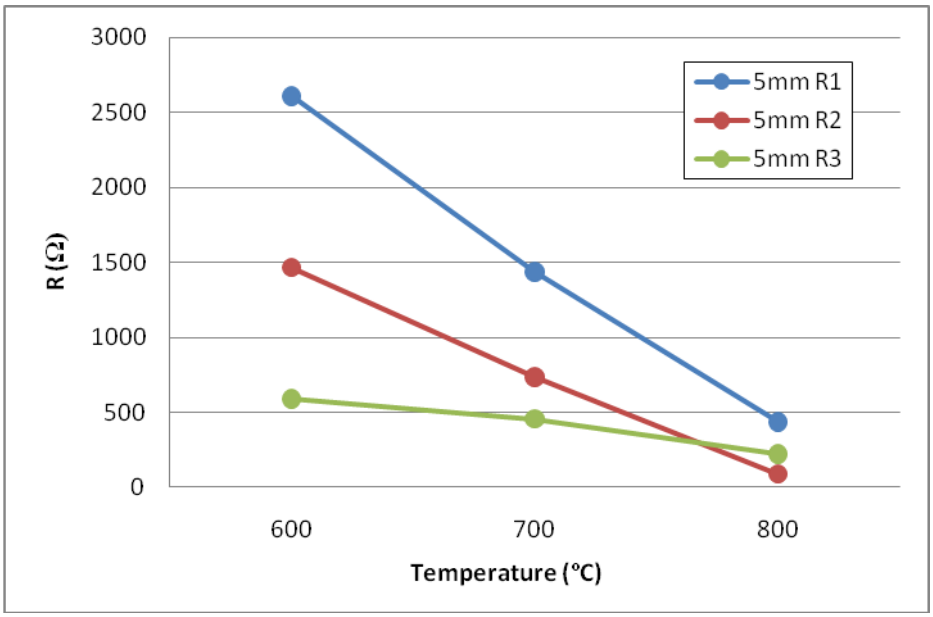

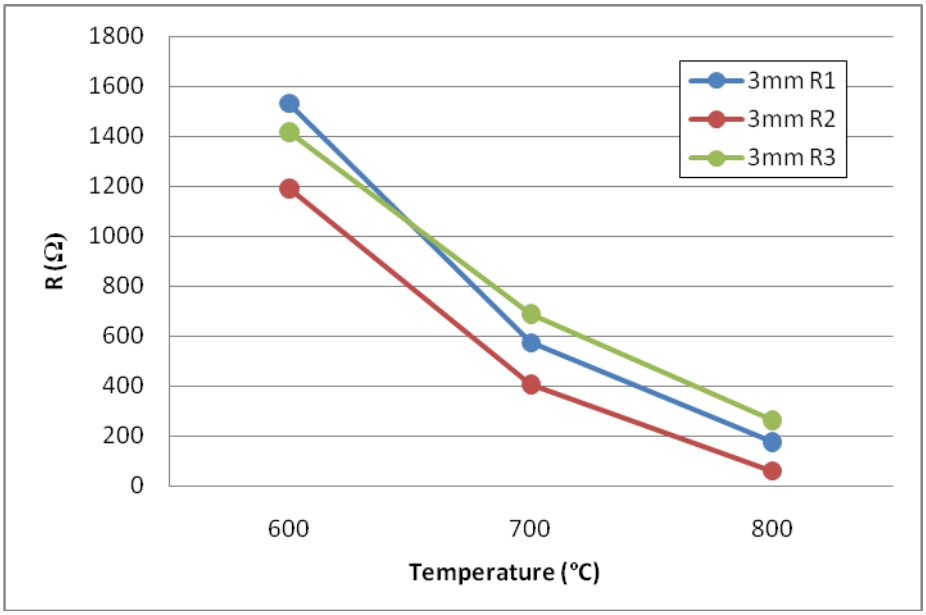

Figure 3.9: Resistance values for the 5 and 3 mm samples

It can be seen that the resistances associated with the 5 mm sample are greater than those of the 3 mm sample. This observation is inconsistent with literature values, which show that resistance decreases as a function of electrode area[4]. This discrepancy could be a result of two phenomena: cracking or lateral electrode resistance. It is possible that during the thermal cycling which occurred during measurements, the differential thermal expansion between the BSCF and YSZ could have resulted in cracks in the electrode. The occurrence of such crack could mean that the measured impedance is only for part of the electrode, instead of the entire electrode, as desired. An additional concern is that the lateral resistance to electron flow inherent to thin films of BSCF is large, meaning the electrode just cannot conduct electrons the full radial distance of the electrodes used in this study. This could also similarly result in decreased effective electrode area. In order to remedy both of these possible causes, a layer of porous silver paint can be applied to the surface of the electrode to distribute the electron transfer across the entire surface, and ensure electron flow throughout the entire electrode.

In addition, it is difficult to correlate the individual elements with processes occurring within this system. While it is fairly certain that the first resistance value (R1) is related to the impedance of the YSZ substrate, the relationships of the other resistance and capacitance values is unknown. In order to determine these relationships, it is necessary to perturb the system and repeat measurements. For instance, if a highly resistive layer is deposited at the BSCF-YSZ interface and a specific feature in the data increases, it can be suggested that this feature corresponds to the impedance at the interface. Due to the nature of processing during sputtering, this technique perfectly lends itself to fabricating samples with such perturbations.

Through this method, insight can be gained on the relationship between the additional resistances and capacitances with electrochemical processes occurring within this system.

Chapter 4

CONCLUSIONS AND FUTURE WORK

Through this research, BSCF powder was successfully synthesized using traditional powder processing methods and its crystal structure was verified using XRD. The BSCF powder was then pressed and sintered into a consolidated, dense target for use in sputter deposition. By depositing multiple BSCF films onto silicon under a variety of sputtering powers, gas pressures and gas compositions, the optimal processing parameters were determined.

After these conditions were determined, BSCF was deposited onto a YSZ substrate in order to model an SOFC system. Using a mask, 200 mm thick circular electrodes ranging from 1 to 5 mm in diameter were deposited on the front of the substrate, while a 9.5 x 9.5 mm square counter electrode was deposited on the back of the substrate.

Using a novel impedance spectroscopy setup, measurements were taken on this sample. Initial measurements were taken on 5 and 3 mm samples at 600, 700 and 800°C. The Baumann R/C network for MIEC perovskites was applied to this sample, but the fits were highly inaccurate. Instead a more universal circuit was applied to obtain more accurate fit results.

Based on the XRD results of deposited films, the phase of the films is unclear. Because BSCF relies on the perovskite crystal structure for conduction, the poor conductivity measurements could be due to non-crystallinity of the film. If the deposited films are indeed amorphous, or contain amorphous regions, depositing films

at high temperature could induce crystallization. A technique called glancing-angle x-ray diffraction (GAXRD) can be applied to characterize the crystal structure of the thin films.

Increased resistance could also be due to microcracking that occurred in the BSCF film due to thermal stresses that it experienced during impedance measurements or due to high lateral electron resistance. Each would result in measuring a decreased effective electrode area. In order to measure the performance of the entire electrode, it is possible to take measurements after coating the electrodes with a layer of porous silver paint, which would distribute electron transfer over the entire free surface of the electrode.

This work was successful in synthesizing dense, thin-film BSCF electrode samples which can be used to model an SOFC system. While initial impedance spectroscopy measurements used to characterize this system did not correspond with literature results, a great deal was learned about the system which gives insight into improving the processing and measurement techniques in the future.

APPENDIX

Table A.1: Raw thickness results from optical interferometry measurements

Sample ID	2-6	2-3	3-5	3-3	1-8	1-5	4-5	4-2	6-2	6-5	5-5	5-2
Power [W]	25	25	25	25	50	50	50	50	75	75	75	75
Pressure [mTorr]	5	10	5	10	5	10	5	10	5	10	5	10
Ar:O2 ratio	9:1	9:1	8:2	8:2	9:1	9:1	8:2	8:2	9:1	9:1	8:2	8:2
Top [nm]	30.03	38.3	37.73	30.71	58.4	57.92	77.84	53.1	80.8	84.8	50	107.2
Middle [nm]	29.8	35.47	44.57	27.35	56.8	55.9	83.3	58.99	80	96.8	50.4	102.4
Bottom [nm]	33.56	35.45	40.61	28.59	56	57.35	82.75	53.34	80	95.2	51.4	104

Table A.2: Raw fit results for impedance spectroscopy measurements

	Temp [°C]	R1 [Ω]	R2 [Ω]	R3 [Ω]	CPE1 [F]	CPE1-a [#]	CPE2 [F]	CPE2-a [#]
5mm	600	2611	1465	587.4	8.30E-05	0.63	4.19E-04	0.97
	700	1437	733.1	455.9	3.82E-05	0.64	9.64E-05	0.90
	800	434.7	88.08	219.1	9.59E-05	0.61	8.41E-05	0.79
3mm	600	1532	1192	1418	1.56E-04	0.50	4.09E-04	0.86
	700	574.3	406.7	688	1.02E-04	0.54	1.79E-04	0.77
	800	175.6	59.5	262.5	3.04E-04	0.46	4.13E-04	0.62

Figure A.1: 65 mm (~2.5 in) stainless-steel die press set

Figure A.2: X-ray diffractometer (PANalytical X'Pert Powder Diffractometer)

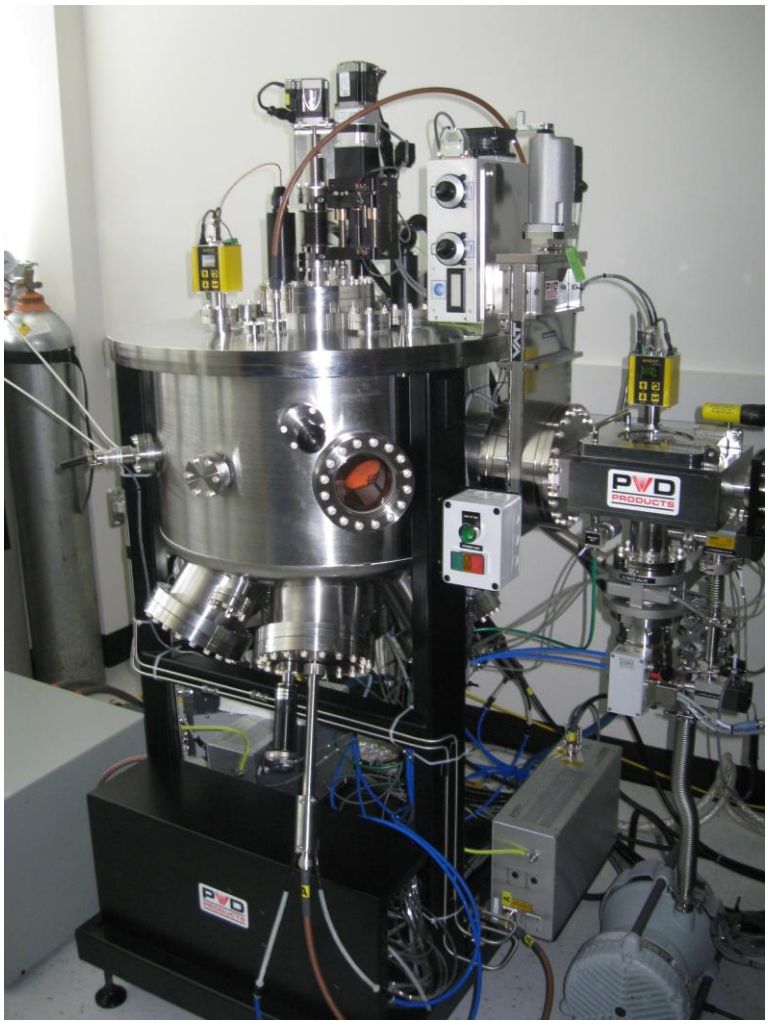

Figure A.3: Sputtering system (PVD Products)

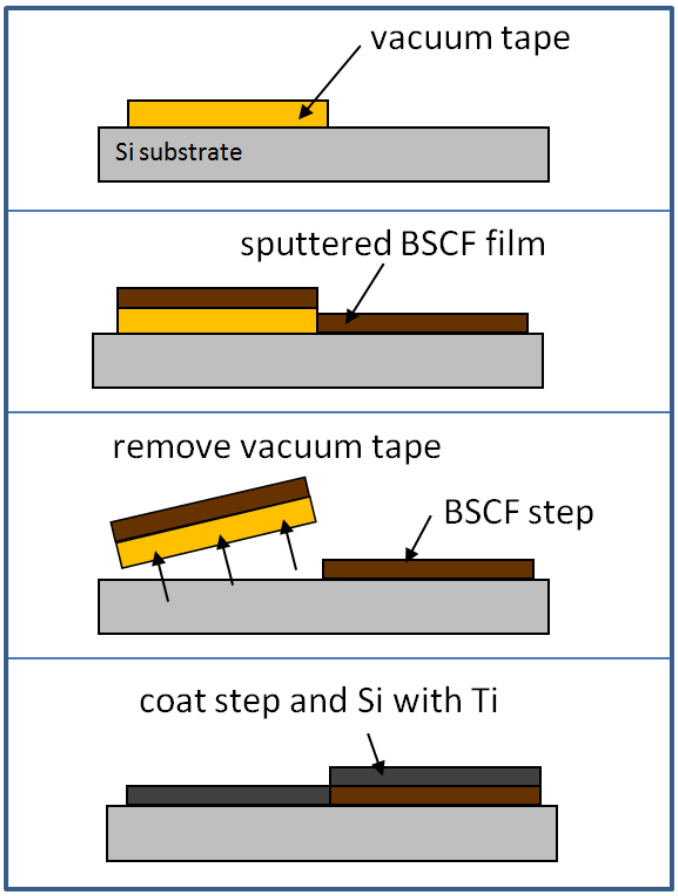

Figure A.4: Steps in preparing sample for deposition measurement

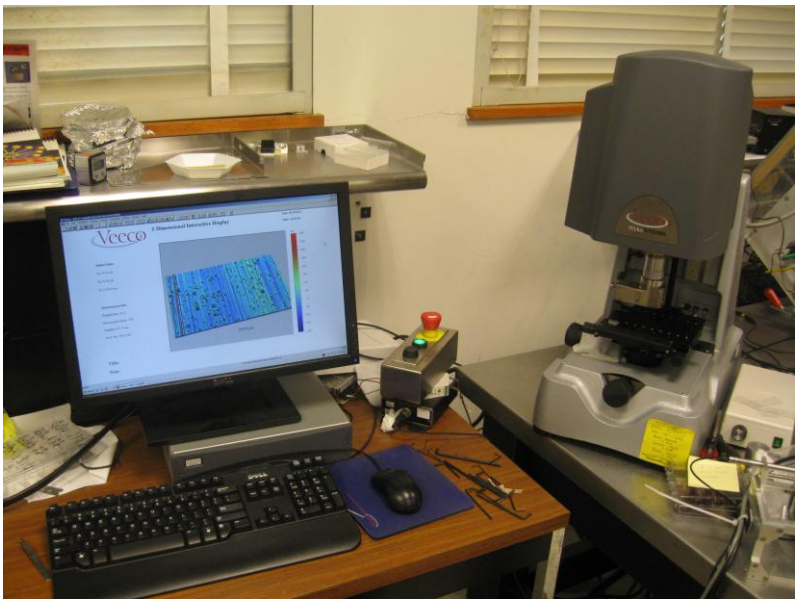

Figure A.5: Optical interferometer (Veeco Wyko NT9100)

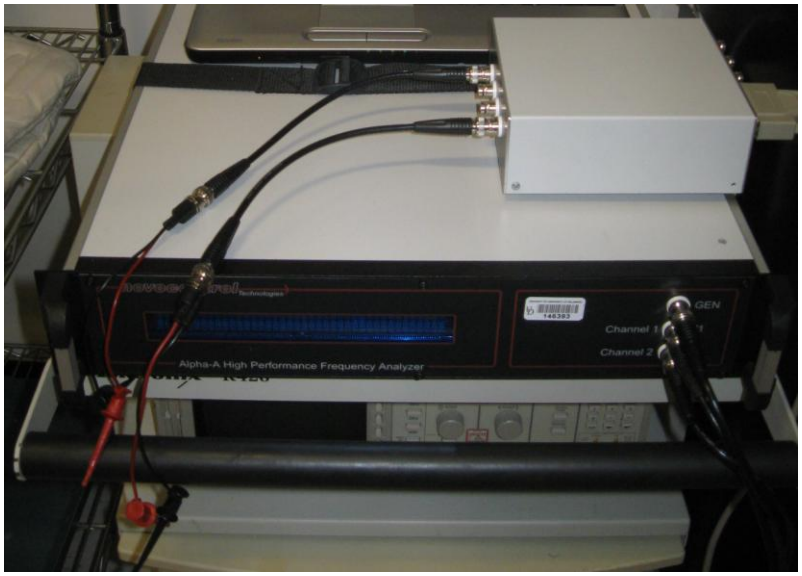

Figure A.6: Impedance analyzer (Novocontrol Alpha-A impedance analyzer with a ZG-4 test interface for 2-wire measurements)

REFERENCES

1. N. Q. Minh, *Journal of the American Ceramic Society* **76**, 563-588 (1991).
2. J.L. Hertz and H. L. Tuttle, *Journal of the Electrochemical Society* **154**, B413-B418 (2007).
3. Z. Shao and S. M. Haile, *Nature* **433**, 170-173 (2004).
4. F. S. Baumann, J. Fleig, H.-U.. Habermeier, J. Maier, *Solid State Ionics* **177**, 1071-1081 (2006).
5. F. S. Baumann, J. Fleig, H.-U. Habermeier, J. Maier, *Solid State Ionics* **177**, 3187-3191 (2006).
6. J.-W. Lee, Z. Liu, L. Yang, H. Abernathy, S.-H. Choi, H.-E. Kim, M. Liu, *Journal of Power Sources* **190**, 307-310 (2009).
7. B. Wei, Z. Lu, S. Li, Y. Liu, K. Liu, W. Su, *Electrochemical and Solid-State Letters* **8**, A428-A431 (2005).
8. M. Burriel, C. Niedrig, W. Menesklou, S. F. Wagner, J. Santiso, E. Ivers-Tiffee, *Solid State Ionics* **181**, 602-608 (2010).